STATE OF THE CLIMATE IN 2020

7. REGIONAL CLIMATES

P. Bissolli, C. Ganter, T. Li, A. Mekonnen, and A. Sánchez-Lugo, Eds.

Special Online Supplement to the *Bulletin of the American Meteorological Society* Vol.102, No. 8, August, 2021

https://doi.org/10.1175/2021BAMSStateoftheClimate_Chapter7.1
Corresponding authors:
North America: Ahira Sánchez-Lugo / Ahira.Sanchez-Lugo@noaa.gov.
Central America and the Caribbean: Ahira Sánchez-Lugo / Ahira.Sanchez-Lugo@noaa.gov
South America: Ahira Sánchez-Lugo / Ahira.Sanchez-Lugo@noaa.gov
Africa: Ademe Mekonnen / amekonne@ncat.edu
Europe: Peter Bissolli / Peter.Bissolli@dwd.de
Asia: Tim Li / timli@hawaii.edu
Oceania: Catherine Ganter / Catherine.Ganter@bom.gov.au
©2021 American Meteorological Society
For information regarding reuse of this content and general copyright information, consult the AMS Copyright Policy.

STATE OF THE CLIMATE IN 2020
Regional Climates

Editors

Jessica Blunden
Tim Boyer

Chapter Editors

Freya Aldred
Peter Bissolli
Howard J. Diamond
Matthew L. Druckenmiller
Robert J. H. Dunn
Catherine Ganter
Nadine Gobron
Gregory C. Johnson
Rick Lumpkin
Tim Li
Ademe Mekonnen
John B. Miller
Twila A. Moon
Ahira Sánchez-Lugo
Ted A. Scambos
Carl J. Schreck III
Sharon Stammerjohn
Richard L. Thoman
Kate M. Willett

Technical Editor

Andrea Andersen

***BAMS* Special Editor for Climate**

Michael A. Alexander

American Meteorological Society

Cover credit:
Rights Managed Photo by STR/AFP via ©Getty Images
Flooded buildings are seen in Nanjing, in China's eastern Jiangsu province on 19 July 2020.
Vast swaths of China were inundated by the worst flooding in decades along the Yangtze River.

Regional Climates is one chapter from the *State of the Climate in 2020* annual report. Compiled by NOAA's National Centers for Environmental Information, *State of the Climate in 2020* is based on contributions from scientists from around the world. It provides a detailed update on global climate indicators, notable weather events, and other data collected by environmental monitoring stations and instruments located on land, water, ice, and in space. The full report is available from https://doi.org/10.1175/2021BAMSStateoftheClimate.1.

How to cite this document:

Citing the complete report:
Blunden, J. and T. Boyer, Eds., 2021: "State of the Climate in 2020". *Bull. Amer. Meteor. Soc*, **102** (8), Si–S475, https://doi.org/10.1175/2021BAMSStateoftheClimate.1

Citing this chapter:
Bissolli, P., C. Ganter, T. Li, A. Mekonnen, and A. Sánchez-Lugo, Eds., 2021: Regional Climates [in "State of the Climate in 2020"]. *Bull. Amer. Meteor. Soc.*, **102** (8), S357–S463, https://doi.org/10.1175/2021BAMSStateoftheClimate_Chapter7.1.

Citing a section (example):
Thiaw, W. M., P.-H. Kamsu-Tamo, M. F. Zaheer, and B. Pugh, 2021: Central Asia [in "State of the Climate in 2020"]. *Bull. Amer. Meteor. Soc.*, **102** (8), S441–S445, https://doi.org/10.1175/2021BAMSStateoftheClimate_Chapter7.1

Editor and Author Affiliations (alphabetical by name)

Alfaro, Eric J., Center for Geophysical Research and School of Physics, University of Costa Rica, San José, Costa Rica
Alves, Lincoln M., Centro de Ciencia do Sistema Terrestre/Instituto Nacional de Pesquisas Espaciais, Sao Paulo, Brazil
Amador, Jorge A., Center for Geophysical Research and School of Physics, University of Costa Rica, San José, Costa Rica
Andrade, B., Seychelles Meteorological Authority, Mahe, Seychelles
Argeñalso, Francisco, Centro Nacional de Estudios Atmosféricos, Oceanográficos y Sísmicos, Tegucigalpa, Honduras
Asgarzadeh, P., National Center for Climate and Drought Crisis Management, Islamic Republic of Iranian Meteorological Organization, Iran
Baez, Julian, Universidad Católica Nuestra Senora de la Asunción, Asunción, Paraguay
Barakiza, Reuben, Burundi Hydrometeorological Department, Bujumbura, Burundi
Bardin, M. Yu., Yu. A. Izrael Institute of Global Climate and Ecology; Institute of Geography, Russian Academy of Sciences, Russia
Bardin, Mikhail, Institute of Global Climate and Ecology, Moscow, Russia
Bissolli, Peter, Deutscher Wetterdienst, WMO RA VI Regional Climate Centre Network, Offenbach, Germany
Bochníček, Oliver, Slovak Hydrometeorological Institute, Slovakia
Bukunt, Brandon, NOAA/NWS Weather Forecast Office, Guam
Calderón, Blanca, Center for Geophysical Research, University of Costa Rica, San José, Costa Rica
Campbell, Jayaka D., Department of Physics, The University of the West Indies, Jamaica
Chandler, Elise, Bureau of Meteorology, Melbourne, Victoria, Australia
Chang'a, Ladislaus, Tanzania Meteorological Authority, Dar es Salaam, Tanzania
Cheng, Vincent Y. S., Environment and Climate Change Canada, Toronto, Ontario, Canada
Clarke, Leonardo A., Department of Physics, The University of the West Indies, Jamaica
Correa, Kris, Servicio Nacional de Meteorología e Hidrología del Perú, Lima, Perú
Cortés, Catalina, Dirección de Meteorológica de Chile, Santiago de Chile, Chile
Costa, Felipe, International Centre for Research on El Niño, Guayaqui, Ecuador
Cunha, A.P.M.A., Centro Nacional de Monitoramento e Alertas de Desastres Naturais CEMADEN, Sao Paulo, Brazil
Demircan, Mesut, Turkish State Meteorological Service, Ankara, Turkey
Dhurmea, K. R., Mauritius Meteorological Service, Vacoas, Mauritius
Diawara, A., NOAA/NWS National Centers for Environmental Prediction, Climate Prediction Center, College Park, Maryland
Diouf, Sarah, NOAA/NWS National Centers for Environmental Prediction, Climate Prediction Center, College Park, Maryland
Dulamsuren, Dashkhuu, Climate change and resource research section, Information and Research, Institute of Meteorology, Hydrology and Environment, National Agency for Meteorology, Hydrology and Environmental Monitoring, Ulaanbaatar, Mongolia
ElKharrim, M., Direction de la Météorologie Nationale Maroc, Rabat, Morocco
Espinoza, Jhan-Carlo, Université Grenoble Alpes, Institut des Géosciences de l'Environnement, IRD, CNRS, Grenoble INP, Grenoble, France
Fazl-Kazem, A., National Center for Drought Monitoring and Crisis Management, Islamic Republic of Iranian Meteorological Organization, Iran
Fenimore, Chris, NOAA/NESDIS National Centers for Environmental Information, Asheville, North Carolina
Fuhrman, Steven, NOAA/NWS National Centers for Environmental Prediction, Climate Prediction Center, College Park, Maryland
Ganter, Catherine, Bureau of Meteorology, Melbourne, Victoria, Australia
Gleason, Karin, NOAA/NESDIS National Centers for Environmental Information, Asheville, North Carolina
Guard, Charles "Chip" P., Tropical Weather Sciences, Sinajana, Guam
Hagos, Samson, Pacific Northwest National Laboratory, Department of Energy, Richland, Washington
Hanafusa, Mizuki, Tokyo Climate Center, Japan Meteorological Agency, Japan
Hasannezhad, H. R., National Center for Climate and Drought Crisis Management, Islamic Republic of Iranian Meteorological Organization, Iran
Heim, Jr., Richard R., NOAA/NESDIS National Centers for Environmental Information, Asheville, North Carolina
Hidalgo, Hugo G., Center for Geophysical Research and School of Physics, University of Costa Rica, San José, Costa Rica
Ijampy, J. A., Nigerian Meteorological Agency, Abuja, Nigeria
Im, Gyo Soon, Climate Change Monitoring Division, Korea Meteorological Administration, South Korea
Joseph, Annie C., Dominica Meteorological Service, Canefield, Dominica
Jumaux, G., Météo France, Direction Interrégionale pour l'Océan Indien, Réunion
Kabidi, K. R., Direction de la Météorologie Nationale Maroc, Rabat, Morocco
Kamsu-Tamo, P-H., NOAA/NWS National Centers for Environmental Prediction, Climate Prediction Center, College Park, Maryland
Kennedy, John, Met Office Hadley Centre, Exeter, United Kingdom
Khan, Valentina, Hydrometeorological Research Center of the Russian Federation/A.M. Obukhov Institute of Atmospheric Physics, Russian Academy of Sciences, Moscow, Russia
Khiem, Mai Van, Viet Nam National Center of Hydro-Meteorology Forecasting, Viet Nam Meteorology Hydrology Administration, Viet Nam
King'uza, Philemon, Tanzania Meteorological Authority, Dar es Salaam, Tanzania
Korshunova, Natalia N., All-Russian Research Institute of Hydrometeorological Information - World Data Center, Obninsk, Russia
Kruger, A. C., Climate Service, South African Weather Service, Pretoria, South Africa Lakatos, Mónika, Climatology Unit, Hungarian Meteorological Service, Budapest, Hungary
Lam, Hoang Phuc, Viet Nam National Center of Hydro-Meteorology Forecasting, Viet Nam Meteorology Hydrology Administration, Viet Nam
Lander, Mark A., University of Guam, Mangilao, Guam
Lavado-Casimiro, Waldo, Servicio Nacional de Meteorología e Hidrología del Perú, Lima, Perú
Lee, Tsz-Cheung, Hong Kong Observatory, Hong Kong, China
Leung, Kinson H. Y., Environment and Climate Change Canada, Toronto, Ontario, Canada
Li, Tim, Department of Atmospheric Sciences, University of Hawaii, Honolulu, Hawaii, USA
Macara, Gregor, National Institute of Water and Atmospheric Research, Ltd., Auckland, New Zealand
Mamen, Jostein, Climate Division, Norwegian Meteorological Institute, Oslo, Norway
Marengo, José A., Centro Nacional de Monitoramento e Alertas de Desastres Naturais CEMADEN, Sao Paulo, Brazil
McBride, Charlotte, Climate Service, South African Weather Service, Pretoria, South Africa
Mekonnen, Ademe, Department of Physics, North Carolina A & T University, Greensboro, North Carolina
Misevicius, Noelia, Instituto Uruguayo de Meteorología, Montevideo, Uruguay
Moise, Aurel, Centre for Climate Research Singapore, Meteorological Service, Singapore

Editor and Author Affiliations (alphabetical by name)

Molina-Carpio, Jorge, Universidad Mayor de San Andrés, La Paz, Bolivia
Mora, Natali, Center for Geophysical Research, University of Costa Rica, San José, Costa Rica
Mostafa, Awatif E., Department of Seasonal Forecast and Climate Research, Cairo Numerical Weather Prediction, Egyptian Meteorological Authority, Cairo, Egypt
Mtongori, Habiba, Tanzania Meteorological Authority, Dar es Salaam, Tanzania
Mutai, Charles, Kenya Meteorological Department, Nairobi, Kenya
Ndiaye, O., Senegalese Meteorological Service, Dakar, Senegal
Nieto, Juan José, International Centre for Research on El Niño, Guayaqui, Ecuador
Nyembo, Latifa, Tanzania Meteorological Authority, Dar es Salaam, Tanzania
Nying'uro, Patricia, Kenya Meteorological Department, Nairobi, Kenya
Pan, Xiao, Nanjing University of Information Science and Technology, China
Pascual Ramírez, Reynaldo, National Meteorological Service of Mexico, Mexico City, Mexico
Phillips, David, Environment and Climate Change Canada, Toronto, Ontario, Canada
Pugh, Brad, NOAA/NWS National Centers for Environmental Prediction, Climate Prediction Center, College Park, Maryland
Rajeevan, Madhavan, Earth System Science Organization, Ministry of Earth Sciences, New Delhi, India
Rakotonirina, M. L., Madagascar Meteorological Service, Madagascar
Ramos, Andrea M., Instituto Nacional de Meteorologia, Brasilia, Brazil
Robjhon, M., NOAA/NWS National Centers for Environmental Prediction, Climate Prediction Center, College Park, Maryland
Rodriguez Camino, Ernesto, Agencia Estatal de Meteorología, Madrid, Spain
Rodriguez Guisado, Esteban, Agencia Estatal de Meteorología, Madrid, Spain
Ronchail, Josyane, Laboratoire LOCEAN-IPSL, Paris, France
Rösner, Benjamin, Laboratory for Climatology and Remote Sensing, Faculty of Geography, University of Marburg, Marburg, Germany
Salinas, Roberto, Dirección de Meteorología e Hidrología/Dirección Nacional de Aeronáutica Civil, Asunción, Paraguay
Sánchez-Lugo, Ahira, NOAA/NESDIS National Centers for Environmental Information, Asheville, North Carolina
Sato, Hirotaka, Tokyo Climate Center, Japan Meteorological Agency, Japan
Sato, Hitoshi, Tokyo Climate Center, Japan Meteorological Agency, Japan
Sayouri, Amal, Direction de la Météorologie Nationale Maroc, Rabat, Morocco
Sebaziga, Joseph, Rwanda Meteorology Agency, Kigali, Rwanda
Sensoy, Serhat, Turkish State Meteorological Service, Ankara, Turkey
Spillane, Sandra, Met Éireann, Dublin, Ireland
Trachte, Katja, Brandenburg University of Technology, Cottbus, Germany
van der Schrier, Gerard, Royal Netherlands Meteorological Institute, De Bilt, Netherlands
Sima, F., Division of Meteorology, Department of Water Resources, Banjul, The Gambia
Smith, Adam, NOAA/NESDIS National Centers for Environmental Information, Asheville, North Carolina
Spence, Jacqueline M., Meteorological Service, Jamaica, Kingston, Jamaica
Sreejith, O. P., India Meteorological Department, Pune, India
Srivastava, A. K., India Meteorological Department, Pune, India
Stella, José L., Servicio Meteorológico Nacional, Buenos Aires, Argentina
Stephenson, Kimberly A., Department of Life Sciences, The University of the West Indies, Jamaica
Stephenson, Tannecia S., Department of Physics, The University of the West Indies, Jamaica
Supari, S., Division for Climate Variability Analysis, Center for Climate Change Information, BMKG, Indonesia
Tajbakhsh-Mosalman, Sahar, Islamic Republic of Iranian Meteorological Organization, Iran
Tamar, Gerard, Grenada Meteorological Office, St. George, Grenada
Taylor, Michael A., Department of Physics, The University of the West Indies, Jamaica
Teshome, Asaminew, Ethiopia Meteorological Agency, Addis Ababa, Ethiopia
Thiaw, Wassila M., NOAA/NWS National Centers for Environmental Prediction, Climate Prediction Center, College Park, Maryland
Tobin, Skie, Bureau of Meteorology, Melbourne, Victoria, Australia
Trotman, Adrian R., Caribbean Institute for Meteorology and Hydrology, Bridgetown, Barbados
Van Meerbeeck, Cedric J., Caribbean Institute for Meteorology and Hydrology, Bridgetown, Barbados
Vazifeh, A., National Center for Drought Monitoring and Crisis Management, Islamic Republic of Iranian Meteorological Organization, Iran
Wakamatsu, Shunya, Tokyo Climate Center, Japan Meteorological Agency, Japan
Wang, Wei, Minhang Meteorological Bureau, Shanghai, China
Xin, Fei, Shanghai Climate Center, Shanghai, China
Zeng, F., Pacific Northwest National Laboratory, Department of Energy, Richland, Washington
Zhang, Peiqun, Beijing Climate Center, Beijing, China
Zhu, Zhiwei, Nanjing University of Information Science and Technology, China

Editorial and Production Team

Allen, Jessicca, Graphics Support, Cooperative Institute for Satellite Earth System Studies, North Carolina State University, Asheville, North Carolina
Andersen, Andrea, Technical Editor, Innovative Consulting Management Services, LLC, NOAA/NESDIS National Centers for Environmental Information, Asheville, North Carolina
Hammer, Gregory, Content Team Lead, Communications and Outreach, NOAA/NESDIS National Centers for Environmental Information, Asheville, North Carolina
Love-Brotak, S. Elizabeth, Lead Graphics Production, NOAA/NESDIS National Centers for Environmental Information, Asheville, North Carolina
Misch, Deborah J., Graphics Support, Innovative Consulting Management Services, LLC, NOAA/NESDIS National Centers for Environmental Information, Asheville, North Carolina
Riddle, Deborah B., Graphics Support, NOAA/NESDIS National Centers for Environmental Information, Asheville, North Carolina
Veasey, Sara W., Visual Communications Team Lead, Communications and Outreach, NOAA/NESDIS National Centers for Environmental Information, Asheville, North Carolina

7. Table of Contents

7. Table of Contents

*Please refer to Chapter 8 (Relevant datasets and sources) for a list of all climate variables and datasets used in this chapter for analyses, along with their websites for more information and access to the data.

7. REGIONAL CLIMATES

P. Bissolli, C. Ganter, T. Li, A. Mekonnen, and A. Sánchez-Lugo, Eds.

a. Overview

This chapter provides summaries of the 2020 temperature and precipitation conditions across seven broad regions: North America, Central America and the Caribbean, South America, Africa, Europe and the Middle East, Asia, and Oceania. In most cases, summaries of notable weather events are also included. Local scientists provided the annual summary for their respective regions and, unless otherwise noted, the source of the data used is typically the agency affiliated with the authors. The primary base period used for these analyses is 1981–2010. However, please note that on occasion different nations, even within the same section, may use unique periods to define their normals. Section introductions typically define the prevailing practices for that section, and exceptions will be noted within the text. Similarly, many contributing authors use languages other than English as their primary professional language. To minimize additional loss of fidelity through re-interpretation after translation, editors have been conservative and careful to preserve the voice of the author. In some cases, this may result in abrupt transitions in style from section to section.

b. North America—A. Sánchez-Lugo, Ed.

1) Canada—K. H. Y. Leung, V. Y. S. Cheng, and D. Phillips

In Canada, 2020 was characterized by a warmer-than-average winter in most of southern Canada and southern Nunavut and by a cooler-than-average spring in most of Canada, with the exception of the northern parts of Yukon, Northwest Territories, and Nunavut. The country also experienced a warmer-than-average summer over most of Nunavut and eastern Canada and a warmer-than-average autumn in northern Nunavut. Autumn was cooler than-average across most of western and southern parts of northern Canada.

(I) TEMPERATURE

The 2020 annual average temperature for Canada was 0.3°C above the 1981–2010 average and the 14th-warmest year since nationwide records began in 1948 (Fig. 7.1). Four of the 10 warmest years have occurred during the last decade, with 2010 the warmest year on record (2.2°C above average). The national annual average temperature record has increased 1.8°C over the past 73 years. Spatially, annual anomalies above +0.5°C were recorded in far northern and parts of eastern Canada. Annual anomalies below −0.5°C were observed mainly in the southern areas of Yukon, Northwest

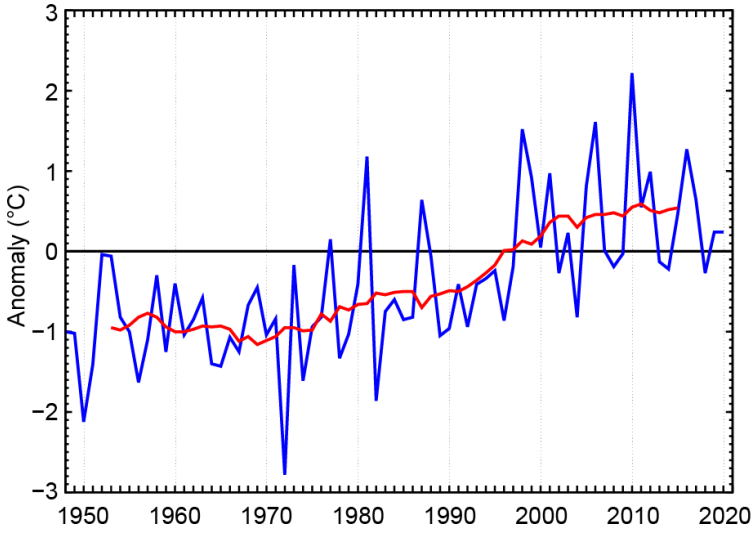

Fig. 7.1. Annual average temperature anomalies (°C; 1981–2010 base period) in Canada for 1948–2020. Red line is the 11-year running mean. (Source: Environment and Climate Change Canada.)

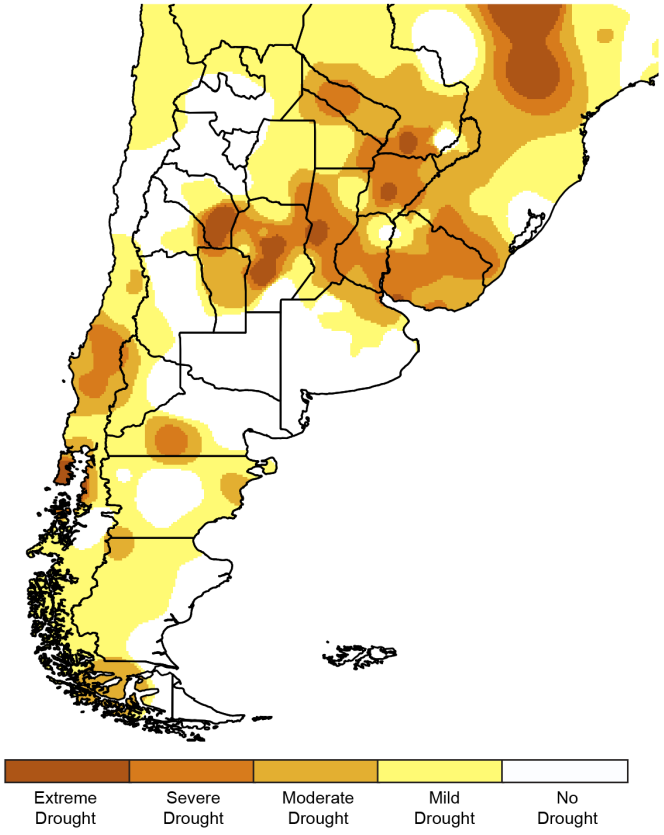

Fig. 7.17. SPI map for the 12-month period Jan–Dec 2020 for southern South America.

and biodiversity. For the year, the Standardized Precipitation Index indicated a classification of severe drought for several locations in Argentina, Uruguay, and also in Chile (Fig. 7.17).

A snowy winter was observed in southern Argentina. Major snowfalls occurred between the end of June and during July, reaching the plateau as well as the coast. Some locations were affected by blocked roads and power outages, among other impacts. According to estimated satellite measurements, the snow cover extent during May–October for central and southern Patagonia was the highest since 2000 (Fig. 7.18).

e. Africa—A. Mekonnen, Ed.

Analyses in this section are based on observational records from meteorological and hydrological services across Africa. Additionally, rainfall data from the Global Precipitation Climatology Project (GPCP) and temperature reanalysis data from the National Centers for Environmental Prediction/National Center for Atmospheric Research (NCEP/NCAR) were also used. Notable events are based on reports from government agencies, research/Early Warning organizations, and United

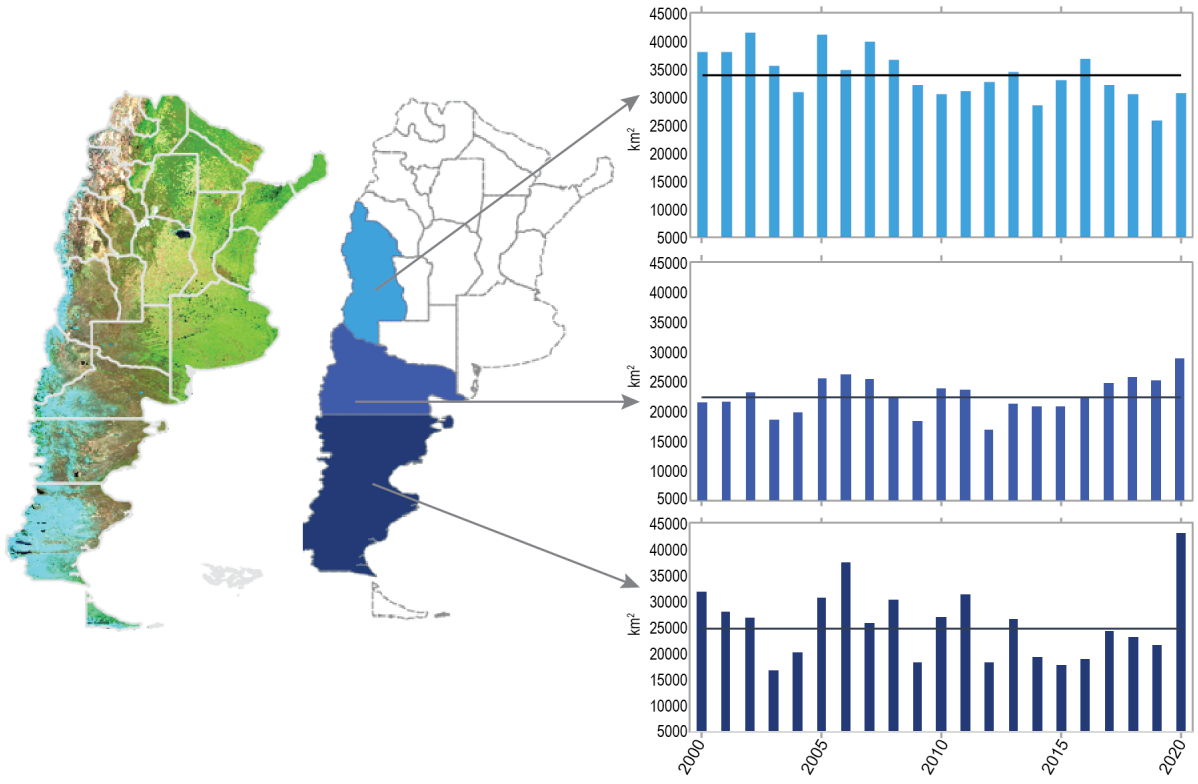

Fig. 7.18. (left) Satellite measurements (MODIS) of snow cover extent (km²; light blue in left-side map) during May–Oct 2020 over central and southern Patagonia. (right) May–Oct snow cover extent (km²) shown in time series for the period 2001–20 for three regions, as depicted on the right-side map.

Nations (UN)-based agencies. The climatological base period used is 1981–2010. Here, temperature and precipitation base periods are referred to interchangeably as average or normal.

In 2020, large parts of northern and equatorial Africa observed above-normal temperatures, while an area centered around the borders between northern Nigeria, southern Niger, and southwestern Chad experienced temperatures up to 1.5°C below normal. Most of South Africa, Namibia, and southern Angola also had below-normal annual temperatures (Fig. 7.19a).

Annual rainfall over the Sahel and eastern Africa, including border areas between Congo and the Democratic Republic of Congo, was above normal. The southern coast of West Africa south of 10°N and most of southern Africa (south of 10°S) received below-normal annual rainfall (Fig. 7.19b).

Extreme weather events and high climate variability were reported across the continent. These include heavy rainfall, extreme flooding, locust infestations, and land-falling tropical cyclones.

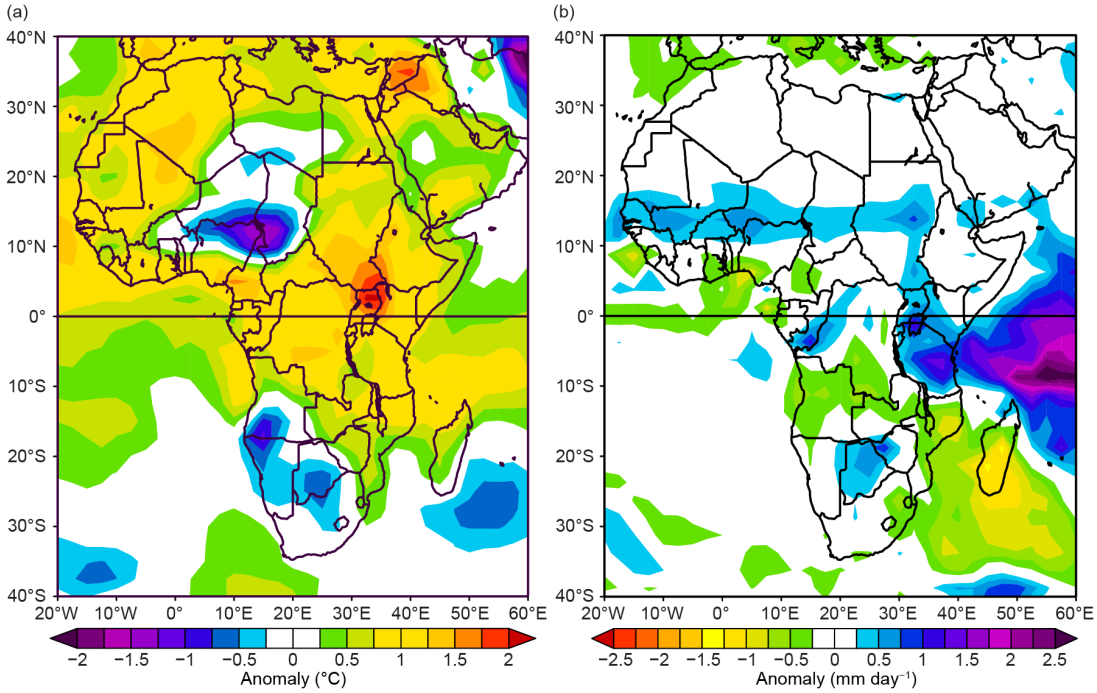

Fig. 7.19. Annual (a) temperature anomalies (°C) and rainfall anomalies (mm day^{-1}) 1981–2010 base period. (Sources: NCEP/NCAR and GPCP.)

1) North Africa—K. Kabidi, A. Sayouri, M. ElKharrim, and A. E. Mostafa

This region, which includes Morocco, Algeria, Tunisia, Libya, Mauritania, and Egypt, is characterized by arid and semi-arid climate. Precipitation over the region is highly variable both in space and time. Rainfall over western North Africa (comprising Morocco and northern and western Algeria) is generally of a short duration but at times intense. Mauritania in the south is characterized by arid to desert climate.

In 2020, above-normal annual mean temperatures dominated most of Mauritania, Morocco, Algeria, and Egypt, while southern Libya observed below-normal temperatures. Moroccan records show that annual temperatures across the country were about 1.2°C above normal, and precipitation was 32% below normal.

(I) TEMPERATURE

Winter (December–February) 2019/20 temperatures were above normal over most of Morocco (+0.9°C), northern Algeria, and Tunisia. Below-normal temperatures were observed over southern Morocco, Mauritania, southern Algeria, Libya, and Egypt (Fig. 7.20a). Temperatures of 1.5° to 2°C below normal dominated southern Libya and southwestern Egypt. Egyptian meteorological

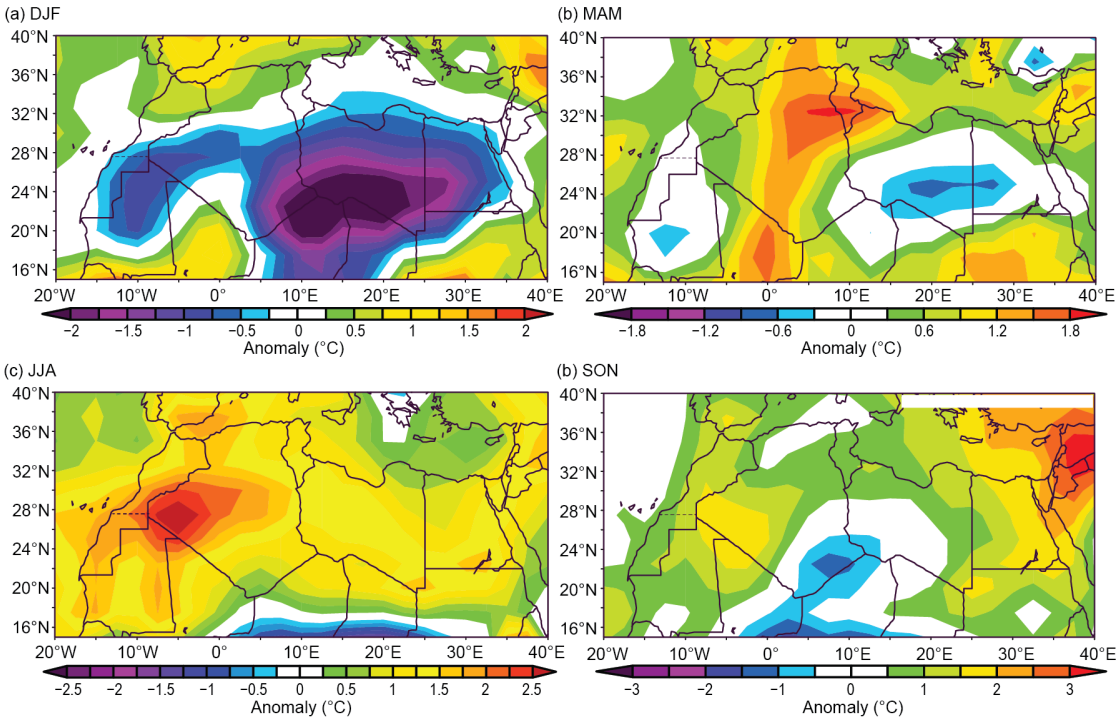

Fig. 7.20. North Africa seasonally averaged mean temperature anomalies (°C; 1981–2010 base period) for (a) DJF 2019/20, (b) MAM 2020, (c) JJA 2020, and (d) SON 2020. (Source: NOAA/NCEP.)

records show above-normal temperatures over the north of the country in December, but January temperatures were as much as 2°C below normal, particularly notable over the southern half. Still, warmth prevailed for the season: a new February temperature record of 3.8°C above normal was recorded at Port Said in northeastern Egypt.

In spring (March–May), temperature anomalies varied across the region (Fig. 7.20b). Above-normal temperatures were observed from northern Mali northward through Algeria, the northern half of Morocco, and Tunisia, while below-normal temperatures were observed to both the west and east of this region (Fig. 7.20b). Stations in the northern mountainous area of Morocco reported monthly maximum temperatures up to 6°C above normal in May (not shown). In Egypt, May was also exceptionally warm, with some stations reporting monthly average temperatures up to 4°C above normal.

Summer (June–August) was warmer than normal throughout the region (Fig. 7.20c). Southeastern Morocco, southwestern Algeria, and northern Mauritania exhibited mean temperature anomalies greater than +2°C. Temperatures exceeding 40°C were reported from Morocco during July and August. High daytime temperatures were also reported from Egypt. For example, 46°C was recorded at Kharga in central Egypt on 31 July. A continuation of above-normal temperatures across Algeria, Morocco, Mauritania, and the eastern half of Egypt (Fig. 7.20d) was observed in autumn (September–November); however, minimum temperatures over Morocco were below normal. Southwestern Libya and southeastern Algeria had mainly below-normal temperatures in autumn.

(II) PRECIPITATION

Generally, precipitation in 2020 was below normal with marked variability across the region and over time. Strong deficits, as much as 90% below normal, were reported from the Saharan region of Morocco. In winter, precipitation was below normal over most of the region (Fig. 7.21a). Morocco reported an overall precipitation deficit up to 56% below normal. Despite an overall winter rainfall deficit, some stations in Egypt reported heavy downpours in January.

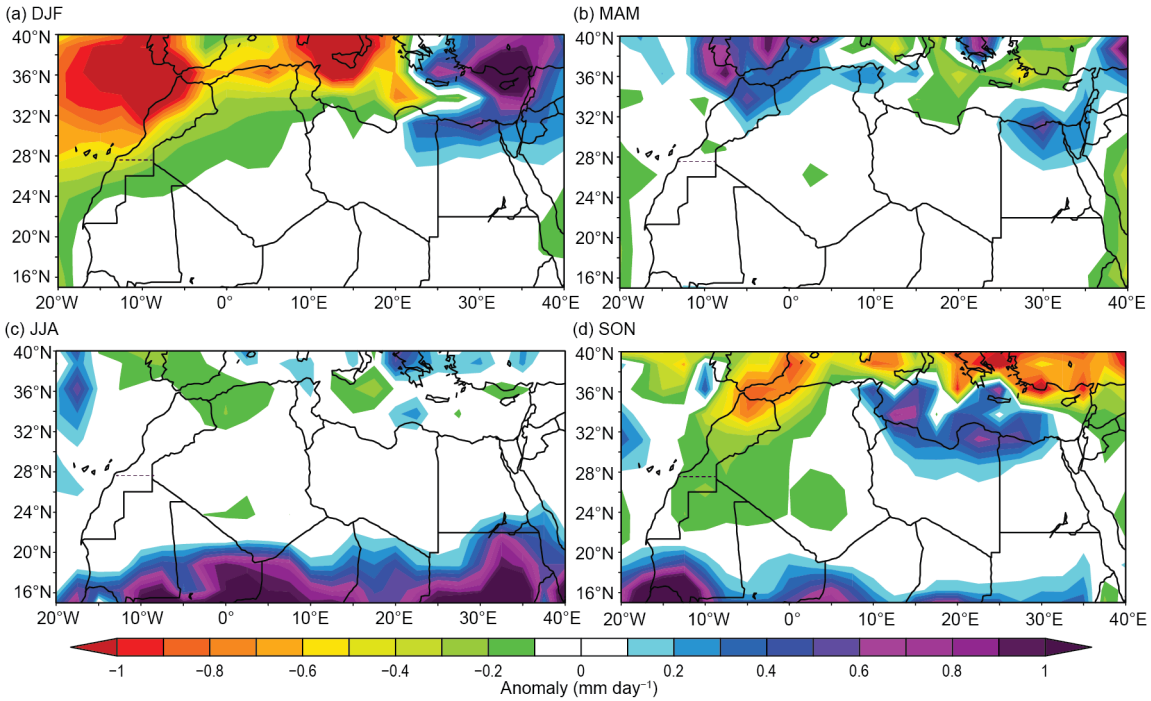

Fig. 7.21. North Africa seasonally averaged rainfall anomalies (mm day^{-1}; 1981–2010 base period) for (a) DJF 2019/20, (b) MAM 2020, (c) JJA 2020, and (d) SON 2020. (Source: NOAA/NCEP.)

Most of northern Morocco, northern Algeria, Tunisia, and Egypt received above-normal rainfall during spring, while the remainder of the region was near normal (Fig. 7.21b). Rainfall in April varied widely across Morocco, with stations reporting between 23% and 265% of normal. In May, Morocco reported 75% above-normal precipitation.

Summer is typically a dry season for North Africa, and the seasonal rainfall was near normal across the region (Fig. 7.21c). In contrast, above-normal rainfall was observed over most of the region during autumn (Fig. 7.21d). Rainfall between 20% and 100% of normal was reported in November from southern and central Morocco. Cairo, Egypt, reported 71 mm of rainfall on 14 November, the highest 24-hour total on record.

(III) NOTABLE EVENTS AND IMPACTS

Reports from Morocco indicated severe flood occurrences during March and November 2020 that caused property damage and cost human lives. Morocco also reported significant damages caused by forest fires that were associated with high summer temperatures, some of which exceeded 40°C in July and August. Similarly high temperatures were observed in Algeria. In Egypt, temperatures reached as high as 46°C at Luxor in the southeast.

2) West Africa—S. Hagos, W. M. Thiaw, Z. Feng, J. A. Ijampy, F. Sima O. Ndiaye, P-H. Kamsu-Tamo, A. Diawara, and S. Diouf

West Africa extends from the Guinea coast to about 20°N and from the eastern Atlantic coast to Niger. Climatologically, it consists of two distinct but inherently linked sub-regions: (1) The Sahel to the north from about 12°N to 17°N, spanning countries from Senegal and The Gambia in the west to Niger in the east and (2) the Gulf of Guinea to the south from about 4°N to 10°N encompassing the Guineas to the west along the east Atlantic coast and Nigeria and Cameroon to the east. The Sahel is semi-arid, while the Coast of Guinea region has a wet tropical climate. The West African monsoon season is associated with the latitudinal movement of a section of the active convective zone associated with the Saharan heat low in the north and its northerly reach limited by Harmattan winds from the northeast. The wet period runs from June through September.

Interannual variations of this seasonal rainfall are controlled by sea surface temperature (SST) fluctuations across the Gulf of Guinea the Mediterranean Sea, and the equatorial east Pacific. At longer timescales, the Atlantic multidecadal oscillation (Martin and Thorncroft 2014) and tropical Indian Ocean SSTs (Giannini et al. 2003) are known to modulate Sahel precipitation. Through most of summer 2020, El Niño–Southern Oscillation (ENSO) conditions were neutral and trending toward La Niña, while the Gulf of Guinea was slightly cooler than normal, both of which typically favor wet conditions over the Sahel region (Janicot et al. 2001; Zhang et al. 2021).

(l) TEMPERATURE

The highest mean annual temperatures, between 27°C and 30°C, were observed over the central and western Sahel, encompassing Senegal, southern Mauritania, Mali, and Burkina Faso (Fig. 7.22a). The area along the border of northeastern Senegal and Mauritania recorded mean annual temperatures exceeding 32°C. Mean annual temperatures were lower over the Gulf of Guinea region, between 24°C and 26°C, over the central areas from Guinea to Benin and much of Nigeria. Mean annual temperatures were about 27°C along the Gulf of Guinea coast and over the northern areas of Cote d'Ivoire, Ghana, Togo, and Benin, extending into northwestern and northeastern Nigeria. Maximum temperatures between 40°C and 46°C were reported from stations in Nigeria between March and June. About 80 days of maximum temperatures exceeding 40°C were reported from Nuguru, Nigeria, surpassing its previous record of 77 days in 2019.

Mean annual temperatures were above normal over much of the western and central Sahel and along the Guinea coast, with departures of about +0.5° to +1°C (Fig. 7.22b). Western Mali, southeastern Senegal, western Guinea, and coastal Gulf of Guinea registered mean annual temperatures above their 90th percentiles (not shown). Mean annual temperatures were below normal over northern Benin and Nigeria and in southern Niger by as much as –1.5°C (Fig. 7.22b), with the lowest temperatures in the past 30 years recorded in northeastern Nigeria. Annual maximum temperatures were overall below normal across the Sahel but exceeded 38°C in southern Mauritania, central Mali, and portions of northwestern and northeastern Niger (not shown). In the Gulf of Guinea, annual maximum temperatures ranged from 24° to 30°C (+1° to +3°C above normal). Annual minimum temperatures were above normal in much of West Africa, with the highest departures from the mean about +2° to +3°C over eastern Senegal and western Mali (not shown).

In 2020, April, May, and June were the warmest months in the Sahel, with readings exceeding 37°C in northern Mali and southern Mauritania, which was +1° to +2°C above normal for Mali and +3°C for southern Mauritania. Mean maximum temperatures exceeded 42°C in northern

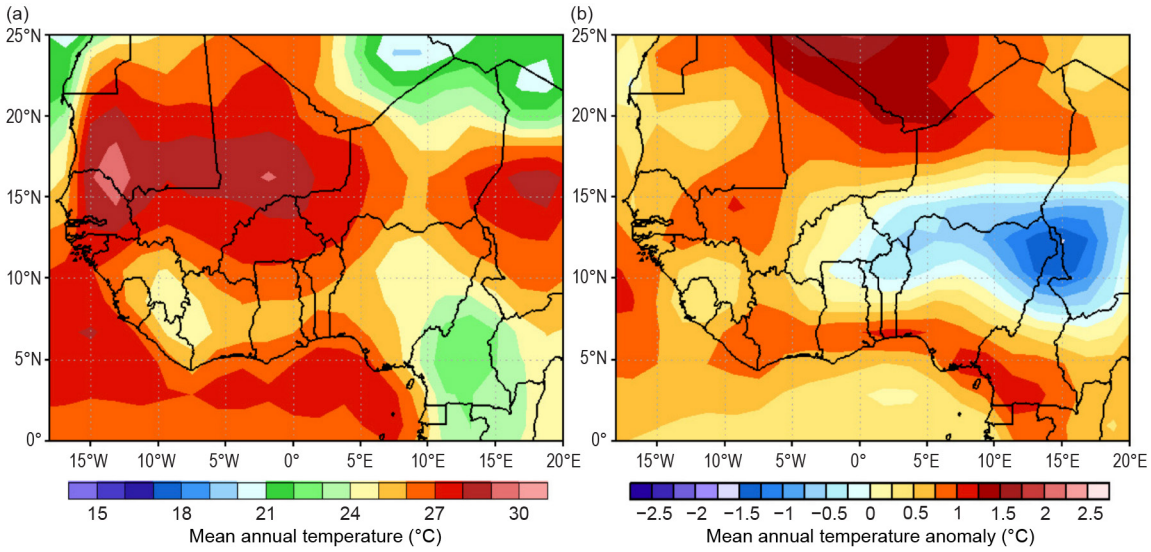

Fig. 7.22. Mean annual (a) temperature and (b) temperature anomalies (°C; 1981–2010 base period) for West Africa in 2020. (Source: NOAA/NCEP.)

Sahel during this time, while mean minimum temperatures were 22° to 26°C. Temperatures were also significantly above normal across West Africa during December 2020, with departures from the mean averaging +2° to +4°C across southeastern Senegal and the western areas of Mali and Burkina Faso. This was due to both elevated maximum and minimum temperatures during the month. Mean monthly temperatures were below normal over the central Sahel, including Burkina Faso, southern Niger, and northern Nigeria during July–September, with temperatures 24° to 26°C, about –1° to –2°C below the mean. The border between Niger and Nigeria observed its lowest mean July temperatures over the past 30 years.

(II) PRECIPITATION

Annual rainfall ranged between 1000 mm and 2000 mm over the Gulf of Guinea region with the areas of maximum rainfall along the western Guinea coast and over southeastern Nigeria (Fig. 7.23a). Rainfall decreased northward, ranging from 300 to 1000 mm in the southern and central Sahel. The climatologically dry areas of the Sahel registered rainfall between 50 mm and 300 mm (Fig. 7.23a). Consistent with the trend of the last 2 decades and the prominence of the Atlantic Multidecadal Oscillation featuring a warm tropical North Atlantic, annual rainfall was once again above normal across the Sahel (Fig. 7.23b; e.g., Mohino et al. 2011), with surpluses of 100–150 mm from Senegal eastward to Niger and exceeding 150 mm over the western areas of Mali and Niger (Fig. 7.23b). These large rainfall departures placed much of the Sahel above its 90th percentile, with west central Senegal and southern Niger recording rainfall above the 95th percentile. Departures of +50 to +100 mm above normal were observed across the northern Sahel.

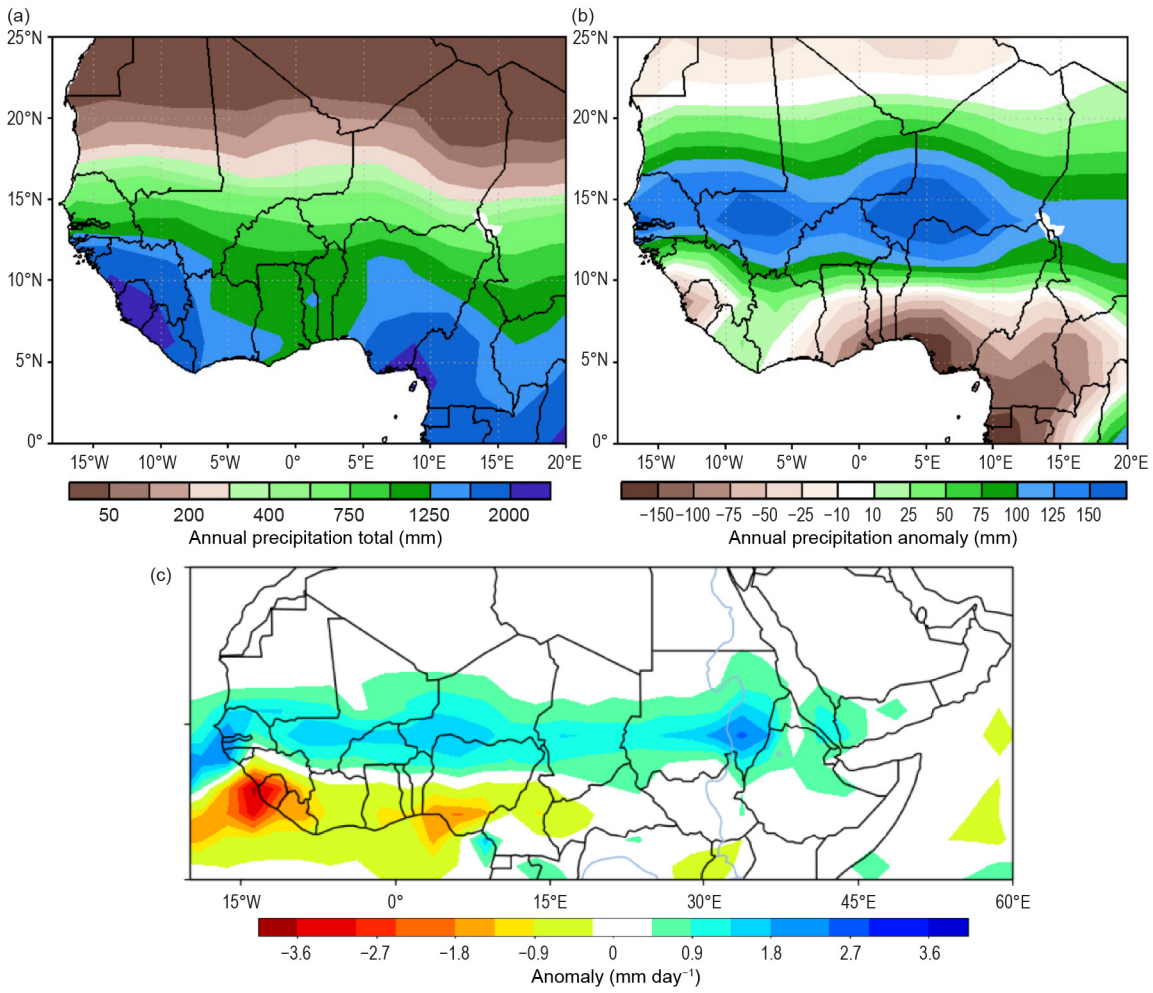

Fig. 7.23. Cumulative annual (a) precipitation totals (mm), (b) annual precipitation anomalies (mm), and (c) Jun–Sep precipitation anomalies (mm day^{-1}) for West Africa in 2020. (Source: NOAA/NCEP and GPCP.)

Over the Gulf of Guinea region, annual rainfall was much below normal along the eastern Guinea coast, with deficits as much as 150 mm below the mean along coastal Nigeria (Fig. 7.23b). Rainfall deficits were 50–150 mm farther inland in the southern areas of Ghana, Togo, Benin, and Nigeria. Mean annual rainfall was slightly below normal over southern Guinea and Sierra Leone and was slightly above normal over Liberia and the northern Gulf of Guinea region.

In the Sahel, rainfall during June–September accounts for much of its annual cumulative rainfall. Totals ranged from 100 to 500 mm in the northern Sahel (just north of 15°N) to 500–1000 mm in the central areas (12°–15°N) to over 1200 mm in the areas of maximum precipitation, including the western Guinean coast. These amounts corresponded to above-normal rainfall across the Sahel, with moisture surpluses exceeding 200 mm across the southern Sahel from Senegal eastward to Niger. The western areas of Niger and Senegal registered rainfall above their 95th percentiles during July–September. Precipitation was significantly below normal over the Sahel in June when much of the precipitation was limited to coastal regions. The situation improved and wetter conditions were observed through the rest of the season for much of West Africa with somewhat drier-than-normal conditions along the Guinean coast (Fig. 7.23c). In Nigeria, 1-day rainfall totals of at least 100 mm were observed in different parts of the country. The city of Yelwa recorded the highest daily rainfall value of 176.2 mm in August followed by Ilorin (160.0 mm), Lafia (152.0 mm), Jalingo (148.4 mm), Bauchi (133.2 mm), and Ibadan (132.0 mm). The month of September contributed significantly to rainfall surpluses in the western Sahel, with over 300 mm (100 mm above the mean) over Senegal, following a drier-than-normal August.

In the Gulf of Guinea region, rainfall was significantly above normal along the western Guinea coast during March–May and October–December, with surpluses of about 100 mm and 200 mm, respectively. In contrast, July–September departures were about 200 mm below the mean in the southern areas and reached 400 mm below the mean over Sierra Leone and Liberia.

(III) NOTABLE EVENTS AND IMPACTS

Extremely heavy rains in West Africa caused many of the countries to face their most devastating floods in recent history. Heavy downpours with accumulations near 100 mm in June soaked southern Niger, resulting in floods across the sub-region. The towns of Maradi and Tahoua were the hardest hit, with 13,667 and 4173 people affected, respectively, according to the Ministry of Humanitarian Action and Disaster Management. As of 21 July, there were 14 fatalities and more than 35,000 people affected and over 3400 houses destroyed, with loss of livestock and crops. Sustained torrential rains in August and September (the station at Gaya in southwestern Niger recorded 130 mm from 23–29 August) caused the Niger River to overflow, shutting down the capital, Niamey. An additional 170 mm between 31 August and 17 September worsened the flood situation as the Niger River rose to approximately 8 m, well above the 6.2-m alert level. According to the government of Niger, as of the end of September, the floods affected about 400,000 people, caused 65 deaths, and severely damaged or destroyed 32,000 houses and 6000 ha of farmland. On 24 August, floods killed three people and displaced 1500 residents in N'Djamena, Chad, according to the International Organization for Migration.

Exceptionally heavy rains across northern and southern Nigeria in late September and early October resulted in widespread floods, compounding the risks to human health and food security. The Benue and Niger Rivers overflowed and caused severe floods in many states, including Kebbi, Niger, Kwara, Kogi, Edo, Anambra, Delta, Kano, Jigawa, Rivers, Bayelsa, and Adamawa. According to the Red Cross, these floods were a result of heavy rainfall in river catchments, coupled with the release of dams in the neighboring countries of Niger, Cameroon, and Benin, which all experienced flooding. In Nigeria, at least 40 people lost their lives. Jigawa State had its worst flood in 32 years, according to the Jigawa State Emergency Management Agency and the International Federation of the Red Cross and Red Crescent Societies (http://floodlist.com/africa/nigeria-floods-october-2020).

On 8 June, a windstorm and heavy rainfall affected parts of Borno State in northeastern Nigeria, causing damage to shelters in several Internally Displaced People's (IDP) camps, according to the International Organization for Migration. The severe weather also affected around 1200 people and damaged a total of 240 shelters in IDP camps in Jere, Damboa, Konduga, and Maiduguri. The heaviest rainfall occurred in Damboa, Konduga, and Maiduguri, resulting in damage to about 60 shelters (Floodlist, 11 June 2020). Yobe state was also affected by the windstorm.

In early June, torrential rain in Accra, Ghana, led to major flooding and two fatalities, according to the National Disaster Management Organization of Ghana. On 18 June, heavy rains in Abidjan and environs, Ivory Coast, caused flash flooding and landslides that killed 13 people, according to National Office Civil Protection of Ivory Coast.

In Burkina Faso, the northeastern town of Dori registered 298 mm between 30 July and 11 August, resulting in eight fatalities, according to the government of Burkina Faso. The floods were so widespread between July and September that the government declared a state of emergency and released $9 million (U.S. dollars) to help flood victims and repair damaged public infrastructure.

In Mali, persistent heavy rains in June and July caused massive flooding in the south. The towns of Mopti and Sikasso were among the hardest hit, with Sikasso receiving cumulative rainfall of 259 and 230 mm in June and July, respectively. Mopti registered 390 mm in July, including 145 mm during 3–5 July and 78 mm during 30–31 July. According to the UN Office for the Coordination of Humanitarian Affairs, the floods affected more than 13,000 people.

In Senegal, the northern town of Linguere—a climatologically dry area—registered 237 mm during 1–9 September. The rains were widespread across the country, forcing the government to declare a state of emergency on 5 September. The Senegalese Red Cross Society indicated that the unprecedented rains decimated homes and flooded streets, especially in the capital city of Dakar, with more than 3000 people affected.

In The Gambia, as in the rest of the Sahel region, monsoon rains started late but persisted well past the climatological end of the season. The Gambia experienced its heaviest downpour in October. According to The Gambia Red Cross Society and the National Disaster Management Agency, severe flooding occurred in some parts of the country following heavy downpours on 13 October, especially notable within the Kanifing Municipality and West Coast Region. The floods caused major property damage and destruction, displacement, and health hazards associated with flooding. Some farmlands were washed away by the rains, particularly in the North Bank Region. The rainy season was also marked by significant high winds that caused major damage to homes.

3) Central Africa—W. M. Thiaw and P-H. Kamsu-Tamo

Central Africa features a unique climate system marked by a strong spatial variability as it spans a wide area of Africa across both the Northern and Southern Hemisphere (NH; SH). The region analyzed in this section extends from the southern tip of the Democratic Republic of Congo (DRC) northward into central Chad. Longitudinally, the region extends from about 5°E to about 35°E. This analysis includes Cameroon, Chad, Central Africa Republic (CAR), DRC, Congo, Gabon, Equatorial Guinea, and São Tomé and Príncipe.

(I) TEMPERATURE

The mean annual temperature was between 21°C and 25°C across much of the region, except for southern Chad, where temperatures approached 27°C and maximum temperatures were up to 35°C. However, the relatively high temperatures were 2° to 3°C below normal in some localities in southern Chad. Mean temperatures along coastal Gabon and Congo and over northeastern DRC averaged about +0.5° to +1°C above the mean, placing the temperatures in the 90th percentile. Temperatures in local areas in central DRC ranked as high as the 99th percentile (Fig. 7.24a). The months of March–May were the warmest in the northern sector of the region. Mean temperatures

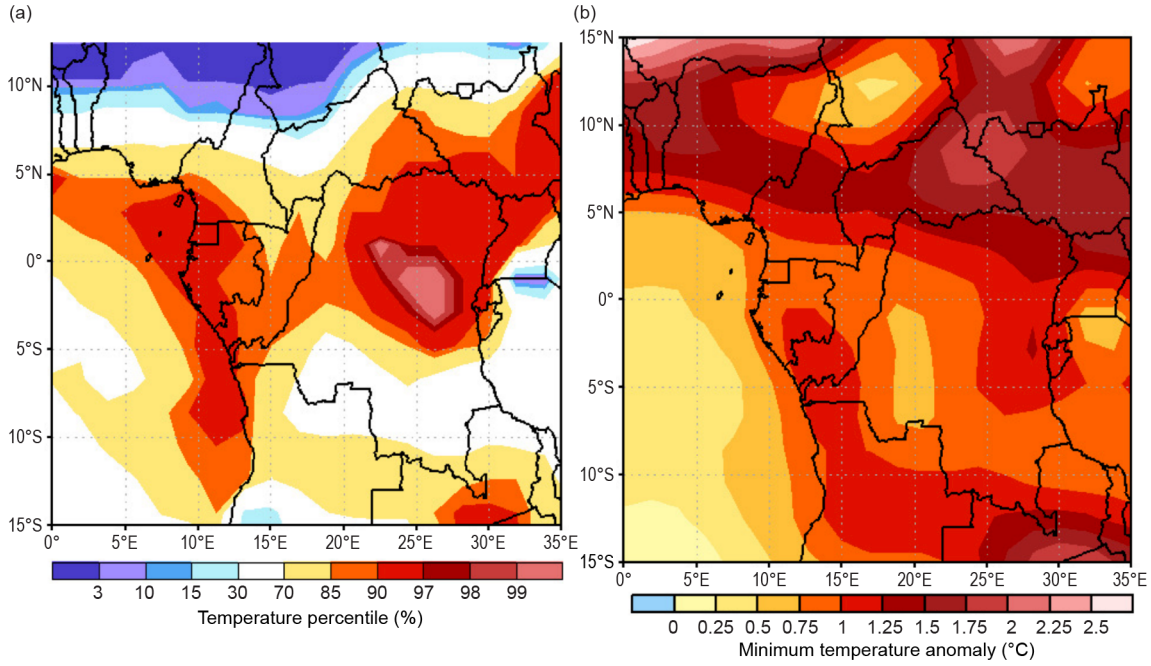

Fig. 7.24. Annual (a) temperature percentiles (%) and (b) minimum temperature anomalies (°C) for Central Africa in 2020. 1981–2010 base period. (Source: NOAA/NCEP.)

were 28° to 30°C across CAR and northern Cameroon. While the temperature exceeded 35°C in some localities in southern Chad in April, this was still about –1°C below the mean. Temperature departures were also –1° to –2°C below the mean in northern Cameroon. Though mean temperatures were relatively low in northern Cameroon and CAR in December, around 20° to 25°C, this area had the highest positive anomalies of about +2° to +3°C above the December mean, placing this month in the 99th percentile. Maximum temperatures for this region in December exceeded 30°C, more than +2°C above the mean and in the 95th percentile. Northern DRC also had maximum temperatures in the 99th percentile during December. Annual minimum temperatures were above normal across the region (Fig. 7.24b). Departures from normal were highest in northeastern DRC, CAR, and northern Cameroon. Minimum temperatures were above normal from January to May, above the 95th percentile in most areas, and were generally normal to below normal from June through November. In December, minimum temperatures were +2° to +3°C above normal in the northern sector encompassing CAR, Cameroon, and southern Chad to end the year.

(II) PRECIPITATION

The climate of Central Africa exhibits seasonality at both the north and south ends of the region. The rainfall pattern is closely related to the north–south movement of the peak convective zone. Rainfall is unimodal in the northern areas of the region and marked with dry conditions during the NH autumn, winter, and spring months of November through April and a return to the rains during the NH summer. The southern areas of the region are dry during the NH summer months and wet during the NH autumn through winter and early spring seasons. The central areas of the region around the equator receive rainfall year-round. The area of maximum annual rainfall is located along coastal Cameroon, with totals exceeding 2000 mm. On average, rainfall amounts range from 1200 mm over the southern tip of DRC and the southern areas of CAR and Cameroon to 2000 mm across much of DRC, Congo, Gabon, and southern Cameroon (Fig. 7.25a). Annual rainfall totals are generally lower over southern Chad with a steep north–south gradient indicated by about 200 mm rainfall amounts in the central areas of Chad to about 1000 mm in the southern tip (Fig. 7.25a).

During 2020, three areas of maximum annual rainfall over southwestern Cameroon and north-central DRC emerged with totals exceeding 2000 mm (Fig. 7.25a). Most areas in northern DRC received rainfall near 2000 mm, while totals ranged from 500 to 1500 mm in the south–north

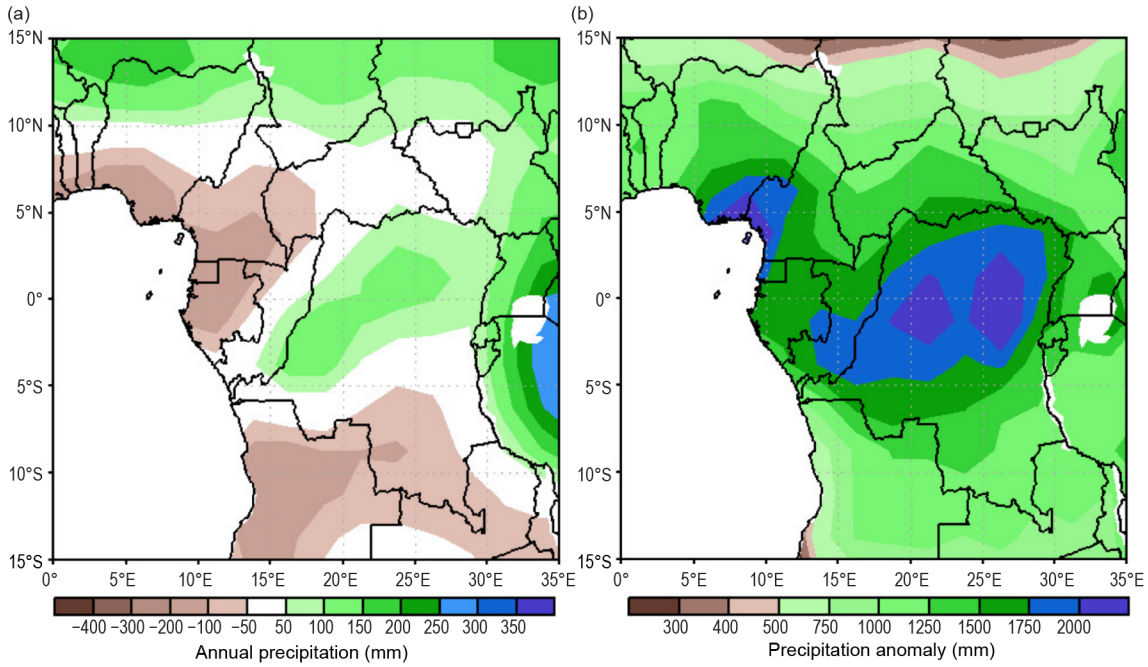

Fig. 7.25. Annual (a) cumulative precipitation (mm) and (b) precipitation anomalies (mm) for Central Africa. 1981–2010 base period. (Source: NOAA/NCEP.)

direction from southern to northern DRC and in the north–south direction from southern Chad to northern DRC and Congo. Rainfall was below normal over western CAR, the southern half of Cameroon, Equatorial Guinea, and much of Gabon, with deficits of 100 to 200 mm (Fig. 7.25b). Annual totals ranked below the 5th percentile along the border between CAR and Cameroon, making 2020 the third-driest year since the start of the record in 1979. Part of the northern DRC observed rainfall about 100–200 mm above normal, placing this area above the 70th percentile. Tshopo Province in northern DRC recorded its second-highest rainfall amount since 1979.

Rainfall was significantly below normal over much of Cameroon and western CAR during the NH summer, with deficits reaching 150 mm in August, in the 5th percentile, making August 2020 one of the driest in this area on record. Rainfall was also below normal over the southern areas of DRC during the NH winter with a 5th-percentile ranking for the January–March period. Totals averaged 300–500 mm, with rainfall deficits more than 150 mm below the mean. Rainfall was much above normal in Chad during July–September, with departures from the mean exceeding 150 mm and above the 80th percentile. A similar pattern prevailed in the central sector of the region during the NH autumn, with areas in east central DRC near the Rwandan border registering about 1000 mm during October–December. The month of November contributed about 500 mm, ~150 mm above the mean and in the 95th percentile, making this month one of the wettest Novembers in the historical record.

(III) NOTABLE EVENTS AND IMPACTS

Heavy rainfall exceeded 135 mm in the South Kivu Province, eastern DRC, during 16–17 April according to the NOAA/CPC satellite rainfall estimates version 2 (RFE2). This deluge triggered extensive flooding, affecting nearly 75,000 people with 40 fatalities and 6000 households displaced, according to the U.S. Agency for International Development.

About 100 mm of rain on 1 October soaked the town of Sake near Lake Kivu in the North Kivu Province of eastern DRC, causing severe flooding and overflowing banks of the Mutahyo River. The provincial government reported at least 11 fatalities, with houses washed away and school and health buildings damaged. Bridges were destroyed and roads washed out, cutting connections between Sake and the provincial capital, Goma.

Heavy rainfall exceeding 120 mm, accompanied by strong winds, on 30 November led to severe flooding in the city of Mbanza-Ngungu in Kongo-Central Province in DRC, causing 13 fatalities and several more injuries, along with destroyed or severely damaged homes.

4) East Africa—L. Chang'a, E. Bekele, W. M. Thiaw, C. Mutai, A. Teshome, P. Nying'uro, J. Sebaziga, H. Mtongori, R. Barakiza, P. King'uza, and L. Nyembo.

East Africa, or the Greater Horn of Africa (GHA), spans the equator and extends between 10°S–20°N and 20°–50°E. Its northern sector comprises Sudan, South Sudan, Ethiopia, Eritrea, Djibouti, and the northern two-thirds of Somalia. Southern Somalia, Kenya, northern Tanzania, Uganda, Rwanda, and Burundi are in its equatorial sector, while the southern sector encompasses central and southern Tanzania. The region has a complex terrain, with elevation ranging from about 160 m below sea level at Ethiopia's northern exit of the Rift Valley to more than 5000 m above sea level at glaciated Mount Kilimanjaro. The complex topographical features of the region are further typified by the presence of large lakes (e.g., Lake Victoria). The complex topography coupled with large-scale forcing factors including the peak moist convective zone (traditionally referred to as the intertropical convergence zone), ENSO, and Indian Ocean dipole are largely responsible for stronger spatial and temporal variability of climate patterns. The lower-latitude regions, including Kenya, Uganda, southern Ethiopia, and southern parts of Somalia and northern Tanzania, experience two rainy seasons during March–May (MAM) and October–December (OND). Central, western, and northern Ethiopia, Sudan, and South Sudan have a single dominant rainy season during June–September (JJAS). Central and southern Tanzania experiences a single dominant rainy season during November–April.

(I) TEMPERATURE

Annual mean temperatures over much of the Sudan, Somalia, Djibouti, Eritrea, and parts of eastern Ethiopia exceeded 30°C, while annual mean temperatures over most of central Ethiopia were less than 22°C (Fig. 7.26a). However, anomalously higher mean annual temperatures were observed western Ethiopia, Kenya, and Uganda (Fig. 7.26a). Annual mean maximum temperatures reached 42°C locally in eastern Sudan and ranged between 35°C and 40°C in other parts of the country. Eastern Kenya and much of Somalia, Djibouti, and Eritrea had annually averaged maximum temperatures between 35°C and 38°C, while it was less than 30°C over western Ethiopia and in the Lake Victoria region.

Meteorological station data indicate that most of the region experienced above-normal temperatures; Addis Ababa Bole International Airport in Ethiopia, for example, reported an annual temperature that was 1.3°C above normal (Fig. 7.26b). Overall, the mean annual temperature for East Africa exhibits a warming trend, with 2020 tied with 2017 as the third-warmest year on record (Fig. 7.26c). Spatially, the annual mean temperature was among the top 5% warmest since 1981 over several locations, including South Sudan, much of Ethiopia, Uganda, and Kenya (Fig. 7.26b).

Anomalously warm temperatures were observed across most of the region between March and December 2020, being most pronounced in central and northern Ethiopia. During December–February (DJF) 2019/20 and JJAS, mean temperatures were below normal over southern Sudan, northern South Sudan, and northeastern and southeastern Ethiopia. Temperatures were above normal in western Ethiopia extending southward into the Lake Victoria region, including western Kenya, Uganda, Rwanda, Burundi, and western Tanzania. Temperatures were above normal over much of East Africa during MAM and OND. These observations indicate a non-uniform temperature dynamic in the region during 2020 that may be driven in part by complex and diverse topographical features.

Maximum temperatures were above normal over much of the region, with the highest anomalies located over western areas of Ethiopia and Kenya along the borders of Uganda, South Sudan, and Sudan. The lowest annual mean minimum temperatures (Tmin) of 2020 were observed over

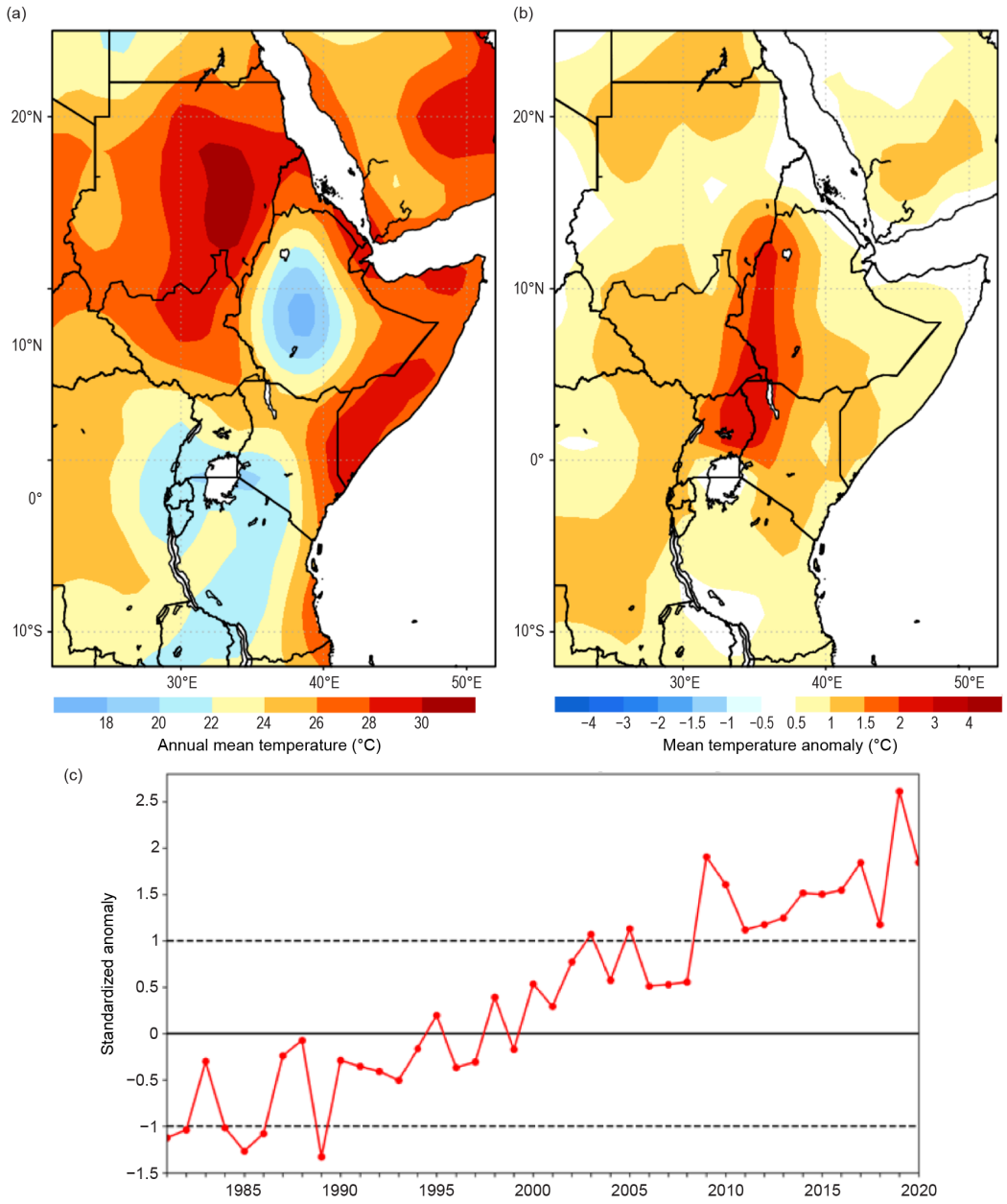

Fig. 7.26. Annual (a) mean temperature (°C) and (b) mean temperature anomalies (°C) for East Africa. 1981–2010 base period. (c) Annual standardized temperature anomaly time series for the period 1981–2020. (Sources: NOAA/NCEP and NOAA CPC.)

western Ethiopia (<8°C) and were between 10°C and 20°C across much of the rest of Ethiopia, southern Uganda and Kenya, and much of Tanzania, except for the coastline (not shown). Mean Tmin were 20°–25°C over much of eastern Sudan, South Sudan, and Somalia. Overall, the Tmin was above normal across the region.

(II) PRECIPITATION

Annual rainfall surpassed 1000 mm across western Ethiopia, portions of South Sudan, much of Uganda, Rwanda, Burundi, western Kenya, and much of Tanzania (Fig. 7.27a). Central and eastern Kenya, central Ethiopia, southern Sudan, and northern South Sudan received rainfall between 600 mm and 1000 mm. Totals were less over northern Sudan, Eritrea, Djibouti, and northern Somalia, with rainfall estimates ranging between 50 mm and 600 mm. Rainfall was significantly above normal over eastern Tanzania, southwestern Kenya, where surpluses exceeded 300 mm (Fig. 7.27b). Rainfall was above normal over much of southern and northwestern Kenya and portions of east central Sudan, with totals averaging 150–300 mm above the mean in eastern

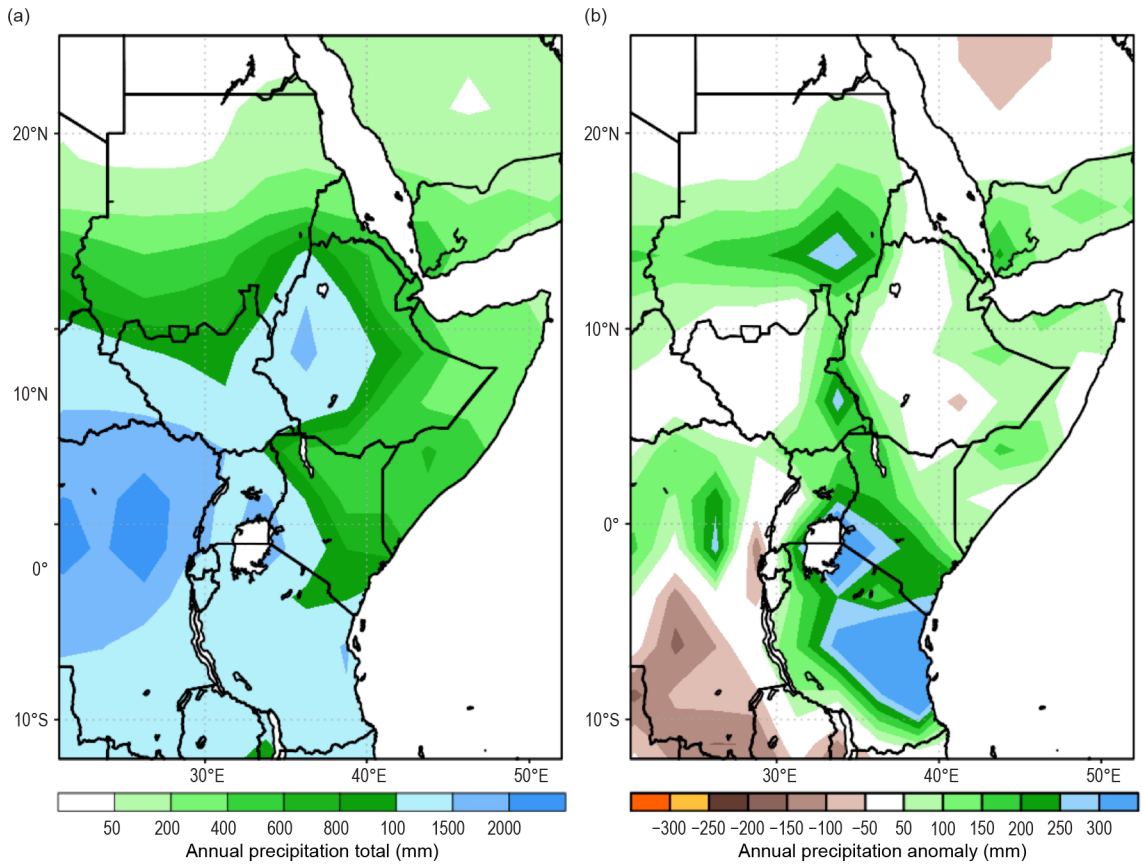

Fig. 7.27. Annual (a) cumulative precipitation (mm) and (b) precipitation anomalies (mm) for East Africa in 2020. 1981–2010 base period; GPCP data. (Source: NOAA/NCEP.)

Uganda and southeastern Sudan. The climatologically drier areas of Somalia, Djibouti, eastern Eritrea, and northern Sudan registered 50–100 mm above the mean. Annual rainfall amount exceeded the 90th percentile over central Tanzania, southwestern Kenya, and much of Sudan. Overall, 2020 was the wettest in the historical record since 1981 in the Lake Victoria region, with totals exceeding 1.5 standard deviations above the mean.

Most of the region recorded normal to above-normal rainfall during all seasons; excessive rainfall was more pronounced during MAM over Burundi, Kenya, Rwanda, Uganda, and Tanzania (not shown). Most of Burundi and Kenya recorded 125%–150% of their long-term means during MAM, while Addis Ababa Bole (Ethiopia) recorded 140% of its normal. Some parts of northwestern Kenya, particularly around Turkana County, recorded more than 200% of its long-term mean precipitation. In Rwanda, both MAM and OND rainfall seasons were relatively higher than the long-term average for most observing stations. In Tanzania, observed rainfall was 150%–175% of normal during November–April and 125%–150% of normal during MAM. Higher rainfall totals exceeding 175% of the long-term average were observed over central and some parts of southwestern Tanzania. Rainfall was also much above normal over Sudan during JJAS, with anomalies exceeding 200 mm locally in the southeast near the border with Ethiopia; rainfall totals across the eastern and central sectors of the Sudan were among their highest (top 5%) since the start of the record in 1981 (Fig. 7.27b).

(III) NOTABLE EVENTS AND IMPACTS

On 23 March, 122.5 mm of rainfall was recorded at the Kilwa meteorological station in Tanzania, the highest on record in this station for the month of March and second highest on record since its record began in 2005. Nearly all dams that supply hydroelectric power in Tanzania were flooded beyond their water-holding capacity such that they were forced to discharge.

April brought extremely heavy rains to East Africa. The most severe downpours occurred during 14–20 April and triggered widespread flooding and landslides in Ethiopia, Somalia, Rwanda, and Burundi. According to NOAA/CPC satellite RFE2, rainfall totals exceeded 160 mm in portions of Rwanda and Burundi during this 7-day period, with more than 200 mm recorded over northern Rwanda. The U.S. Embassy in both countries declared a state of emergency. According to U.S. Agency for International Development and the Government of Rwanda Ministry of Emergency Management, the floods destroyed more than 2000 houses and more than 3500 ha of crops. An estimated 62,300 people were in need of immediate food assistance. There were 113 fatalities and more than 100 injuries due to the extreme rains. In western Burundi, the floods resulted in an overflow of the Ruzizi River, affecting an estimated 45,000 people. Over southern Ethiopia and southern Somalia, rainfall totals during the same period exceeded 200 mm, resulting in flooding with eight fatalities and infrastructural damage, especially in the Gamo region of southern Ethiopia.

On 27 April, 80 mm of rain led to flash flooding that swept through the city of Qardho (also known as Gardo) in the northeastern Bari region of Somalia. At least six fatalities were reported, while hundreds of families lost their homes.

During 2020, extreme events including floods, heavy rainfall, and landslides led to a total of 341 fatalities and more than 13,500 damaged houses in Rwanda, while 7000 houses were damaged and more than 50,000 people were displaced in Burundi. During the OND rainy season in Kenya, there were approximately 300 fatalities and more than 150,000 households were affected due to heavy rainfall and flooding. During the JJAS rainfall season in Ethiopia, more than one million people were affected and nearly 300,000 were displaced due to flooding. In Tanzania, 40 deaths and the destruction of more than 2450 houses were reported due to heavy rainfall and flooding. Similarly, the overflow of the Nile River in Khartoum and the surrounding areas in the Sudan caused extensive damage in property and loss of lives. Elagib et al. (2021) reported that the 2020 floods in the Sudan caused the loss of 417 human lives and affected up to two million people. The flood was associated with heavy rainfall over Ethiopia and upstream Nile basin countries (Elagib et al. 2021).

A widespread desert locust infestation from 2019 into 2020 impacted the equatorial and northern sectors of East Africa, as heavy rains and prevailing winds were favorable for breeding and movement across the region. A large swarm of locusts spread across 14 Kenyan counties and later spread into Ethiopia, northeastern Somalia, Uganda, and South Sudan, while some groups reached parts of northern Tanzania. The massive infestation resulted in significant crop damage across eastern Africa. According to an early assessment by the UN Food and Agriculture Organization, desert locusts caused the destruction of nearly 200,000 ha of cropland and more than 1.2 million ha of pasturelands, as well as the loss of more than 350,000 metric tons of cereal, resulting in one million people in need of food aid in Ethiopia. The World Bank estimated that locust-related losses, including damage to crops, livestock, and other assets, may be as much as $8.5 billion (U.S. dollars) for the East Africa region and Yemen.

5) Southern Africa—A. C. Kruger, C. McBride, M. Robjhon, and W. M. Thiaw

Southern Africa comprises the sub-region located to the south of 5°S and includes Angola, Namibia, Zambia, Botswana, Zimbabwe, Malawi, South Africa, Lesotho, Eswatini, and Mozambique. The region has two main seasons—the wet season, which spans from November of the previous year to April, and the dry season, which lasts from May to October.

(I) TEMPERATURE

Annual mean temperatures were above normal over the northeastern region, with anomalies of about +0.5° to +1°C across eastern Zambia, northern Zimbabwe, Malawi, and northern Mozambique. According to the historical record since 1979, annual temperatures ranked above the 90th percentile in central Zambia, northern Zimbabwe, and northern Mozambique. In contrast,

near- to below-normal temperatures dominated the western and central sectors, including southern Angola, northern Namibia, Botswana, and parts of central South Africa. Southern Angola and northwestern Namibia reported negative anomalies between –1°C and –2°C; this was below the 5th percentile in northwestern Namibia.

Annual maximum temperatures were above normal over northeastern Angola, Zambia, Malawi, northern Mozambique, and parts of western South Africa and southern Mozambique (Fig. 7.28a), while the annual minimum temperature was 0.5° to 2.5°C below normal over southern Angola and northern Namibia (Fig. 7.28b). South Africa reported its fifth-warmest year in the 70-year record, about 0.5°C above normal, based on the data of 26 climate stations (Fig. 7.28c). South Africa is warming at an average rate of +0.16°C per decade, statistically significant at the 5% level.

During DJF 2019/20, mean temperatures were above normal over northern Angola, central Zambia, Zimbabwe, northeastern South Africa, and western and southern Mozambique (not shown). Below-normal temperatures were observed over Botswana and central South Africa. While the average maximum temperature was well below normal over Botswana and central South Africa, it was above normal over a wide area extending from Angola and eastern Namibia eastward to Mozambique.

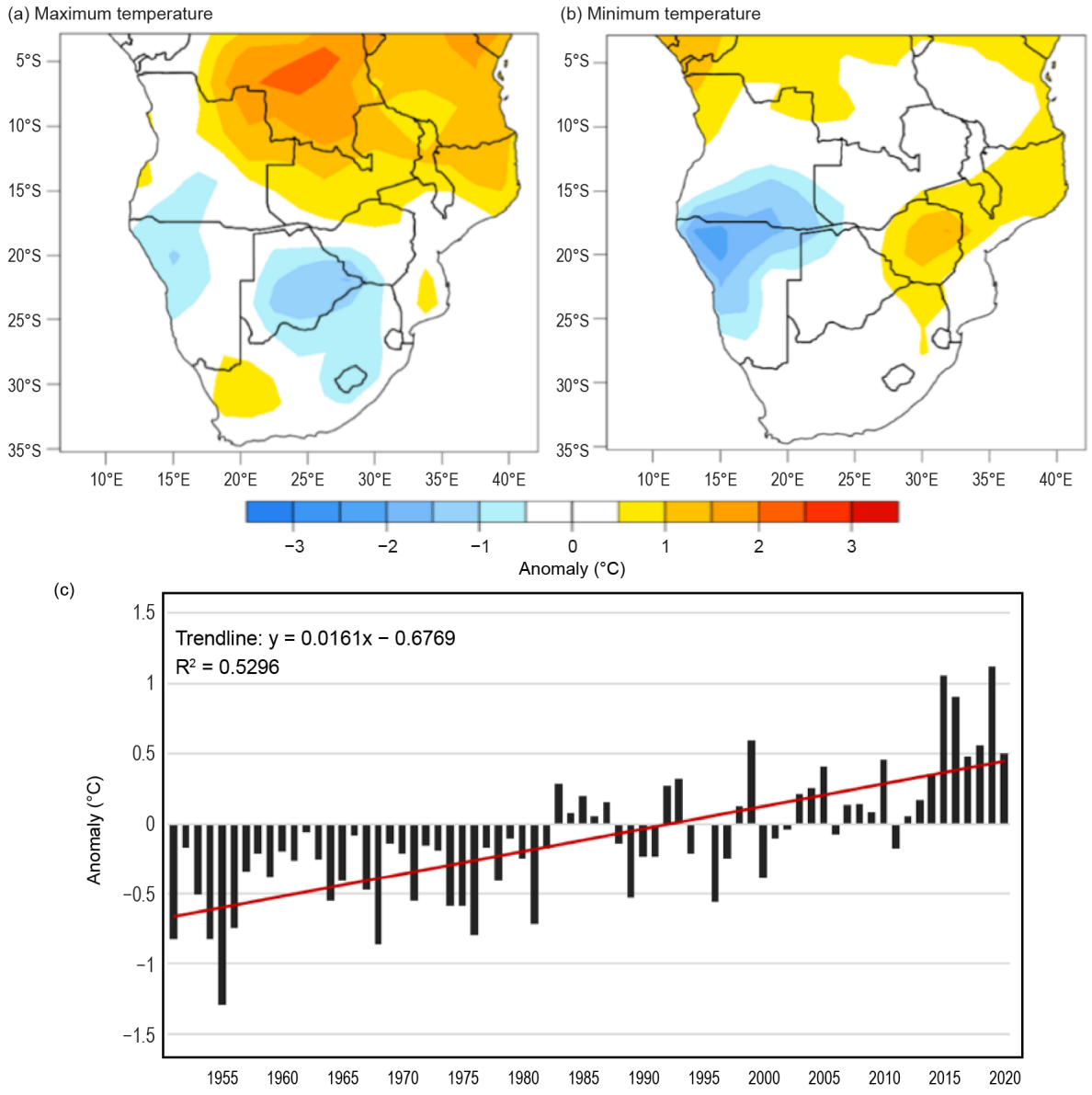

Fig. 7.28. Annual (a) maximum and (b) minimum temperature anomalies (°C; CDAS data). (c) Annual temperature anomaly time series (°C) for the period 1951–2020. Red line indicates linear trend. (Sources: NOAA/NCEP and South African Weather Service.)

During MAM, above-normal temperatures persisted over northern Angola, Zambia, eastern Zimbabwe, Malawi, and parts of northern and southern Mozambique (not shown). During the dry and cold season of JJA, mean temperatures averaged well below normal, with negative anomalies of more than –1.5°C across Angola, northern Namibia, and central South Africa (not shown).

Early during September–November (SON) season, well above-normal temperatures returned over eastern Zambia, Malawi, northern Zimbabwe, and northern Mozambique, while below-normal temperatures lingered in southern Angola and western Namibia (not shown). Maximum temperatures ranked above the 99th percentile over southeastern Zambia, Malawi, and northern Mozambique.

(II) PRECIPITATION

Annual rainfall totals near or above 1000 mm were reported over the northern sector, while accumulations of less than 600 mm were observed across the western region during 2020 (Fig. 7.29a). Rainfall for the year was below normal across much of southern Africa, including Angola, central Zambia, Malawi, northern Mozambique, and western and eastern South Africa, Eswatini, and southernmost Mozambique (Fig. 7.29b). In contrast, annual rainfall was above normal over the central sector, including Botswana, Zimbabwe, and central South Africa. Large rainfall deficits exceeding 250 mm were observed over northeastern Mozambique (Fig. 7.29b). Conversely, surpluses surpassed 250 mm over northeastern Botswana and western Zimbabwe, ranking between the 95th and 99th percentiles, based on the 42-year record.

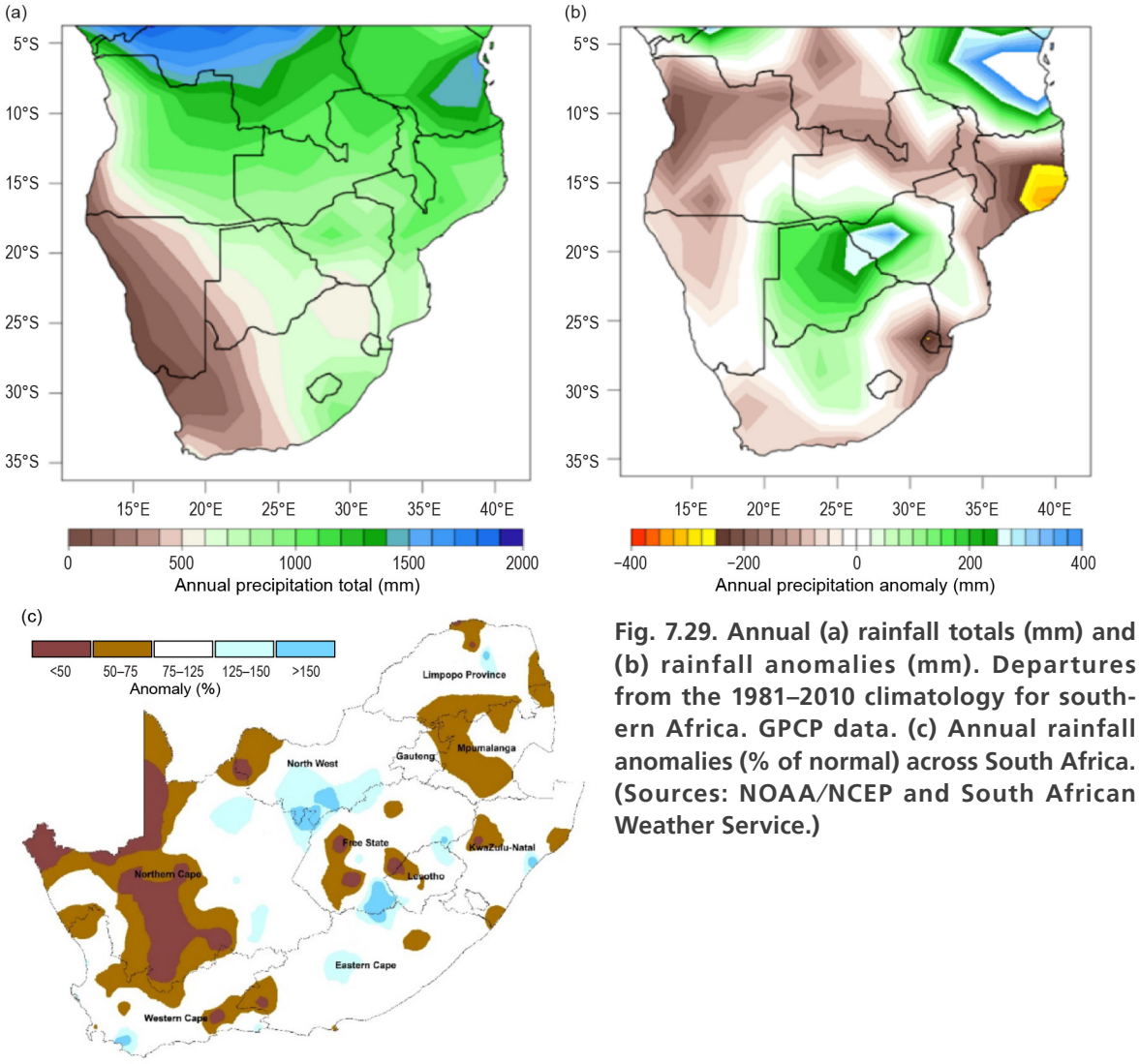

Fig. 7.29. Annual (a) rainfall totals (mm) and (b) rainfall anomalies (mm). Departures from the 1981–2010 climatology for southern Africa. GPCP data. (c) Annual rainfall anomalies (% of normal) across South Africa. (Sources: NOAA/NCEP and South African Weather Service.)

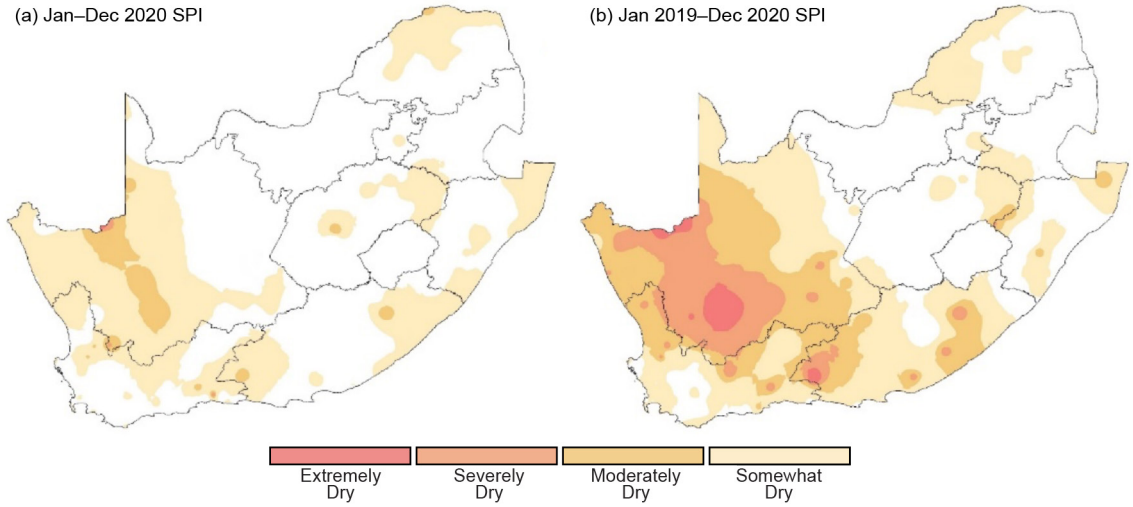

Fig. 7.30. (a) 12-month and (b) 24-month SPI maps for South Africa ending Dec 2020 (Source: South African Weather Service).

The most significant feature of the rainfall during 2020 in South Africa was the persisting dry conditions in western South Africa, with a substantial region receiving less than 50% of its normal precipitation (Fig. 7.29c; see also *Notable events and impacts*). The central interior also shows isolated areas that remained dry. However, the area of South Africa experiencing drought decreased over the year, where some regions received adequate precipitation in the early austral summer rainy season of 2020/21. The remainder of the country received near-normal rainfall. No significant area of the country received substantially above-normal rainfall, except for southern parts of the North–West Province. The 12-month standardized precipitation index (SPI; Fig. 7.30a) for South Africa ending December 2020 indicates that the western interior was somewhat to moderately dry in places; however, the 24-month SPI (Fig. 7.30b) shows that the long-term effects of the drought persist, with extensive regions showing moderate to severely dry conditions over the last 2 years.

During DJF, wetter-than-normal conditions were experienced over western Angola, Botswana, central and northern South Africa, Malawi, and northern Mozambique (not shown), while below-normal rainfall extended over Zambia and northern Zimbabwe to central Mozambique.

During MAM, wetter-than-normal conditions persisted over Botswana, western Zimbabwe, and central South Africa. In contrast, drier-than-normal conditions developed over Angola, Malawi, and Mozambique (not shown). Seasonal accumulation was so low over Malawi and northern Mozambique that rainfall totals were below the fifth percentile.

During the dry season of June–August, rainfall was near normal over much of the region; however, below-normal rainfall was received over Lesotho and southeastern South Africa (not shown). Seasonal rainfall ranked between the fifth and 10th percentiles across central and southern South Africa, suggesting that midlatitude systems likely failed to bring winter moisture into the region. By SON, while near-normal rainfall dominated over much of southern Africa, above-normal rainfall returned over Botswana, southeastern Angola, and southwestern Zambia (not shown). Total rainfall ranked between the 90th and 95th percentiles in northwestern Botswana and southeastern Angola. Conversely, below-normal rainfall re-emerged over southeastern Zambia, northern Zimbabwe, southern Malawi, northern Mozambique, eastern South Africa, Eswatini, and southernmost Mozambique.

(III) NOTABLE EVENTS AND IMPACTS

Dry conditions persisted over large parts of western South Africa during 2020 including some areas where dryness has prevailed for about 7 years. The year began with dry conditions persisting in most parts of the western interior, with above-normal temperatures in the central parts exacerbating the dryness. The Northern Cape was declared a disaster area after drought impacted

the province. A total of 200 million rand (~$14 million U.S. dollars) was set aside to help address the crisis. KwaZulu-Natal Province was also impacted by a shorter-term drought, accompanied by high temperatures, that affected 256 towns and surrounding communities. The most impacted areas include Uthukela, Umzinyathi, Amajuba, Zululand, Uthungulu, and Umgungundlovu districts. Adequate rain fell in the southern and northeastern parts of the country, although some associated severe storms caused extensive damage to infrastructure. By February, above-normal rainfall spread to the central and southeastern interior, but the late-summer rainfall ended abruptly, followed by drier conditions in March. Severe storms were reported in February with extensive damage, especially in the Gauteng and Eastern Cape Provinces. In April some areas received more than twice their normal amounts over the eastern half of South Africa. Localized flooding was reported in several places. Many flooding events occurred during austral summer and autumn. Based on NOAA's CPC RFE2, Gauteng Province received 100–300 mm of precipitation during 4–10 December 2019, which led to flooding in many parts of the Province on 11 December, affecting 3500 people with two fatalities reported, according to the Emergency Events Database (EM-DAT). During 7–10 February, RFE2 estimated 90 mm of precipitation, again in Gauteng, that caused flash floods, leading to three fatalities and affecting 200 people.

According to the Southern African Science Service Centre for Climate Change and Adaptive Land Management, upstream areas, such as Onjiva in southern Angola, recorded cumulative rainfall totals of 263 mm from 26 February to 3 March, which triggered floods over many areas downstream of northern Namibia, including the Oshana, Oshikoto, Omusati, and Ohangwena Regions on 6 March, affecting 1000 people.

During 16–22 March, up to 150 mm of rain fell across northern Zambia, with the largest totals over the Luapula and parts of the Northern Provinces. These large rainfall totals resulted in flooding across 28 districts over the Northwestern, Copperbelt, Luapula, Northern, Muchinga, Eastern, Western, and Lusaka Provinces of Zambia, with an estimated 700,000 people affected, according to the Disaster Management and Mitigation Unit. During the same period, rainfall estimates approached 100 mm over southwest-central Angola, causing flooding and damages and affecting over 2000 families over the Cuanza Sul, Malanje, Lunda Sul, and Cunene Provinces of Angola, based on report from the Agência Angola Press.

Tropical Storm Chalane made landfall over the Muanza District in the Sofala Province of central Mozambique on 30 December, causing at least two fatalities and affecting nearly 11,000 people, according to the United Nations Office for the Coordination of Humanitarian Affairs. The impact was smaller over Zimbabwe as the system weakened into a tropical depression, with about 600 people displaced and minor infrastructure damages reported. In contrast, drought caused food shortage over Lesotho by the end of the year, affecting 766,000 residents, according to EM-DAT.

6) Western Indian Ocean island countries—G. Jumaux, M. Robjhon, W.M. Thiaw, R. Dhurmea, M. L. Rakotonirina, and B. Andrade

The Western Indian Ocean island countries consist of Madagascar, Seychelles, Comoros, Mayotte (France), Réunion (France), Mauritius, and Rodrigues (Mauritius). With two distinct main seasons, western Indian Ocean islands generally experience a warm and wet period during November of the antecedent year to April and a cold and dry season during May–October. Overall, 2020 was warmer than normal (Fig. 7.31). Annual rainfall was above normal in Seychelles and Madagascar and below normal over the rest of the island countries (Fig. 7.31).

(l) TEMPERATURE

The annual mean temperature over Réunion Island (based on three stations) was 0.24°C above normal, the 15th highest since record keeping began in 1968. March and October, both +0.8°C above normal (Fig. 7.32), were among the six warmest for their respective months, while the